RESEARCH ARTICLE

Correspondence to:
J. R. Mioduszewski,
jmiod@scarletmail.rutgers.edu

Attribution of snowmelt onset in Northern Canada

J. R. Mioduszewski[1], A. K. Rennermalm[1], D. A. Robinson[1], and T. L. Mote[2]

[1]Department of Geography, Rutgers University, Piscataway, New Jersey, USA, [2]Climatology Research Laboratory, Department of Geography, University of Georgia, Athens, Georgia, USA

Abstract In the region of Earth most sensitive to climate change, spring snowmelt serves as a measurable indicator of climate change and plays a strong role in the feedbacks that amplify Arctic warming. We characterize the melt season and attribute melt onset in a region of northern Canada during the spring snowmelt season from 2003 to 2011. Melt onset dates are obtained from Advanced Microwave Scanning Radiometer for the Earth Observing System retrievals. Energy balance and meteorological fields are obtained from NASA's Modern Era Retrospective Analysis for Research and Applications product. Analysis of three distinct subregions demonstrates that typical values of energy balance terms vary across the region and have different roles in melt attribution. Melt is controlled more by advective energy farther southwest where melt onset begins sooner, compared to higher levels of radiative energy over the tundra. This study demonstrates that a relatively small region can exhibit large differences in controls on spring snowmelt both within the region and interannually, and these differences can be understood in the context of factors ranging from the large-scale synoptic pattern to land cover and the local energy balance. Being able to attribute melt onset to those drivers that are changing as the high latitudes warm as opposed to those that do not (i.e., insolation) allows better long-term prediction of melt season dynamics and the climatological processes influenced by snow cover and its feedbacks.

1. Introduction

The Arctic climate system has undergone rapid change in the 20th and 21st centuries [*Lemke et al.*, 2007]. This is manifested as accelerating losses in sea ice, glacial mass balance, permafrost, consequent changes throughout the biosphere, and in Northern Hemisphere snow cover extent and duration [*Serreze et al.*, 2007; *Liston and Hiemstra*, 2011; *Camill*, 2005; *Comiso et al.*, 2008; *Hinzman et al.*, 2005]. The marked difference in albedo in snow-covered and bare ground and the trend of earlier snowmelt onset since 1979 [*Foster et al.*, 2008; *Tedesco et al.*, 2009; *Wang et al.*, 2013] is one of the primary drivers of Arctic amplification [*Déry and Brown*, 2007], i.e., observations and modeling showing stronger warming in the Arctic relative to the rest of the Earth System [*Groisman et al.*, 1994; *Serreze and Francis*, 2006]. Therefore, understanding drivers of snowmelt is critical for assessing current trends in snow cover and predicting future responses to Arctic and global change.

As the Arctic warms, terrestrial spring snowmelt has occurred an average of 2 to 4 weeks earlier than it did three decades ago [*Tedesco et al.*, 2009]. June snow cover extent, largely confined to the Arctic, has decreased nearly twice as fast as the well-publicized September sea ice extent during the satellite era [*Derksen and Brown*, 2012], and nearly 50% since 1967 [*Brown et al.*, 2010]. Snow cover across the entire Northern Hemisphere has shown similar earlier snow loss trends responding to warmer temperatures and changes in atmospheric circulation [*Dye*, 2002; *Brown*, 2000; *Déry and Brown*, 2007]. This has been less pronounced over North America than Eurasia [*Dyer and Mote*, 2006; *Brown and Robinson*, 2011], with no trend over the tundra of northern Canada, depending on the data set [*Wang et al.*, 2005]. The regional and monthly differences in these trends suggest that melt drivers may exhibit considerable variability, requiring attribution that adequately resolves these differences.

The most important variables controlling snowmelt are radiative fluxes, energy advection, turbulent heat fluxes, and the temperature departures that synthesize these [*Groisman et al.*, 1994; *Zhang et al.*, 1997; *Aizen et al.*, 2000; *Ohmura*, 2001], but it is unclear whether warmer temperatures primarily drive increased melt, or whether warmer temperatures are a consequence of the earlier melt. It is also uncertain what causes these temperature departures, and temperature departures are not always responsible for earlier melt. Large-scale attribution studies of spring snowmelt have been a challenging undertaking due to the volume of data and its dimensions involved and tend to provide results constrained by this limitation [*Shi et al.*, 2011; *Bamzai*,

2003; *Tedesco et al.*, 2009; *Vicente-Serrano et al.*, 2007]. Regional studies have largely been confined to central and eastern Eurasia [*Aizen et al.*, 2000, 2002; *Shinoda et al.*, 2001; *Ueda et al.*, 2003; *Iijima et al.*, 2006] or western Canada and Alaska [*Bao et al.*, 2011; *Semmens et al.*, 2013]. In contrast, small- and point-scale studies of snowmelt attribution often have the advantage of utilizing detailed energy balance and turbulent flux data at a high temporal resolution [*Sicart and Pomeroy*, 2006; *Stone et al.*, 2002; *Pomeroy and Toth*, 2003; *Marsh et al.*, 2010] but can be difficult to generalize beyond the unique geography of the study location and are often limited to one melt season.

Radiation is the primary mechanism providing energy for snowmelt. Radiative fluxes have been found to play a larger role in melt energy, especially at high latitudes, with advective energy and resultant sensible heat fluxes contributing more to melt at lower latitudes and earlier in the year [*Ohmura*, 2001; *Leathers and Robinson*, 1997; *Zhang et al.*, 1996, 1997]. The greatest control on downwelling longwave (LW) radiation variability during the melt season, however, is considered to be the change in atmospheric moisture content [*Zhang et al.*, 2001], and low cloud cover can raise this radiance by up to $100 \, \text{W m}^{-2}$ [*Stone et al.*, 2002]. *Iijima et al.* [2006] concluded that atmospheric warming and wetting played the greatest role in eastern Siberian snow ablation, with mean water vapor pressure doubling to 4 hPa in the 30 days before the melt onset date. The impact of clouds on snowmelt has been studied extensively [*Bintanja and Van den Broeke*, 1996; *Zhang et al.*, 1996; *Stone et al.*, 2002], with most concluding that low clouds can be responsible for a large contribution to the net radiation balance and subsequent melt. However, averaged over longer time periods, the additional thermal radiation emitted by increased clouds is nearly balanced by the solar energy they block at these latitudes in spring, and this becomes a net cooling effect as the albedo decreases [*Zhang et al.*, 1996; *Dong et al.*, 2001].

The time period in which snow can begin melting is generally understood to be controlled by insolation, whereas interannual variation in this date can be most attributed to variability in downwelling LW radiation [*Zhang et al.*, 2001]. Variability in downwelling LW radiation is largely a function of heat and moisture transport changing the mean atmospheric thickness, as well as cloud cover variations. Synoptic conditions that generate the patterns that control energy advection have been studied on a regional and hemispheric scale. There has been some success correlating winter snow conditions and subsequent melt season timing with teleconnections such as the Arctic Oscillation and Pacific North American pattern [*Tedesco et al.*, 2009; *Bamzai*, 2003; *Brown*, 2000], or simply height fields and modes of atmospheric circulation [*Vicente-Serrano et al.*, 2007; *Stone et al.*, 2002; *Bao et al.*, 2011], but these results depend on the region as well as such methodological considerations as time lags and temporal and spatial averaging. Only few studies explore regional snowmelt drivers by analyzing the local energy balance within the larger synoptic perspective, seeking to build on both small- and large-scale research.

Here the snowmelt onset drivers between 2003 and 2011 in northern Canada are characterized and analyzed by using passive microwave radiometer and atmospheric reanalysis data. Snowmelt onset dates (MOD) were derived from the Advanced Microwave Scanning Radiometer–Earth Observing System (AMSR-E) passive microwave radiometer, while all other data were obtained from Modern Era Retrospective-Analysis for Research and Applications (MERRA), NASA's current state of the art reanalysis product. A range of near-surface energy and atmospheric variables in northern Canada are analyzed at the beginning of the melt season, including 2 m temperature, energy convergence, insolation, specific humidity, and LW cloud radiative effect (CRE). Emphasis is placed on the date of melt onset in three distinct subregions to isolate the primary regional differences. First, validation of the AMSR-E algorithm with station data is provided, and the spatial variability of melt onset times is shown. This is followed by a comparison of energy balance terms to evaluate the importance of each term relative to each other, and how they differ regionally. Attribution of melt is examined primarily by identifying the number of years in each grid cell when each variable exceeds a predefined threshold to separate the contribution of radiation versus synoptic influences. Next, composites of 500 hPa height fields are calculated to show the typical synoptic conditions during melt in each region and gain a sense of the large-scale dynamics that drive the local energy balance. Finally, the earliest and latest melt onset occurrences are analyzed to examine if melt drivers are different in extreme snowmelt years.

2. Study Area

The study region spans 59° to 70°N, 90° to 115°W and is split into three subregions for much of the analysis (Figure 1). As will be shown, these regions have distinctly different energy balance components and are
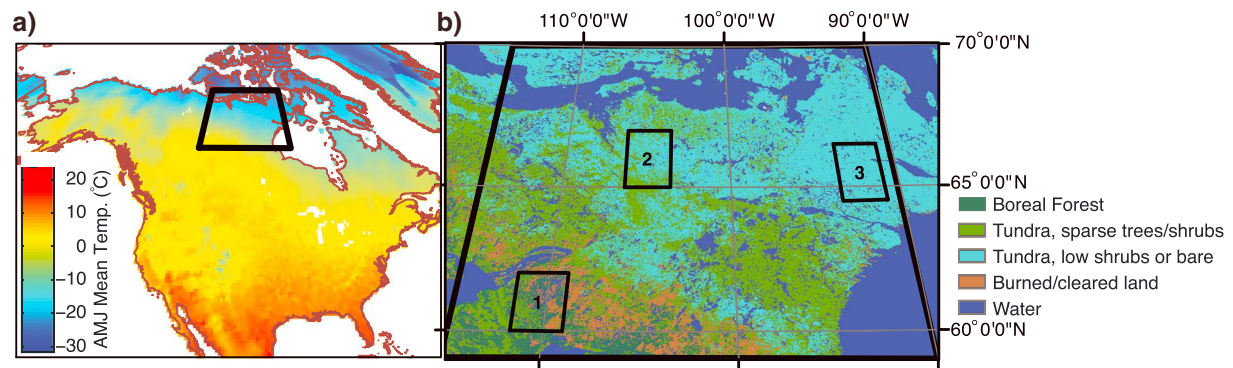
Figure 1. Map of (a) North America showing the study region with mean April–June 2 m temperature (NOAA/NCEP reanalysis) overlaid and (b) land cover map (modified from *Latifovic et al.* [2002]) of the study area with subregions shown in boxes.

therefore useful to contrast the spatial variation within the study area. Seasonal temperature patterns and land cover distribution take on a southwest-northeast orientation, with boreal forest transitioning to tundra (Figure 1). The southwest-northeast orientation of temperature and land cover is likely in part due to the orientation of the Rocky Mountains, which favors a 500 hPa trough near Hudson Bay and a ridge further downstream [*Seager et al.*, 2002]. Lake coverage is more extensive moving north and east into the tundra (Figure 1b), which increases the region's albedo during melt, particularly relative to the boreal forest where snow is removed from dark canopy.

3. Data and Methods

3.1. Melt Onset Algorithm

The occurrence of melt in a grid cell was determined using input from a gridded binary (presence/absence) data set of surface snowmelt that incorporates observations from AMSR-E [*Knowles*, 2006] and the National Ice Center's Interactive Multisensor Snow and Ice Mapping System (IMS) product [*Ramsay*, 1998]. In this data set, a grid cell is designated as experiencing surface melt if the diurnal amplitude variation (DAV) (i.e., the absolute value of the brightness temperature difference between the ascending and descending nodes) exceeds 18 K. The melt identification methodology here is similar to that used in previous studies, which incorporate a minimum DAV criterion and a minimum brightness temperature (Tb) criterion to identify melt [e.g., *Ramage et al.*, 2007]. In this study, only the DAV criterion is used because the maximum Tb threshold used for identification of snow-covered surfaces would be mutually exclusive with the minimum Tb to identify melt.

Snow presence prior to melt onset was identified following the approach used in AMSR-E/Aqua L3 Global Snow Water Equivalent product, where snow was indicated with $Tb36V \leq 255$ K and $Tb36H \leq 245$ K [*Tedesco et al.*, 2004], and using IMS as a supplement. The start of the study period was set to 2003, the first year of AMSR-E observations. While our snowmelt detection algorithm can be used with other passive microwave products, none are identical to AMSR-E, so we derive MOD from one satellite product to avoid errors associated with using several passive microwave products over time. Gaps due to missing satellite imagery are filled using the previous day's data for up to 5 days. This algorithm was validated in section 4.1 over the 2003–2009 period with Baker Lake (64°N, 96°W) and Yellowknife (62°N, 114°W) snow depth and maximum temperature data, obtained from Environment Canada. These stations are representative of the climate across much of the study region's tundra and boreal forest, respectively.

The MOD was determined from the data generated from the above methodology with an algorithm that identifies the date corresponding to the first day of melt in the "primary" melt season without incorporating early melt events, similar to previous studies [e.g., *Wang et al.*, 2013]. MOD is specified if surface melt is indicated for either four or more consecutive days, or three consecutive days and at least twice more in the following 4 days. If melt is not triggered, this condition is relaxed to three consecutive days and one of the following 4 days. The surface melt product was regridded from its original 25 km grid on Equal-Area Scalable Earth projection to $2/3° \times 1/2°$ to be compatible with MERRA data.

3.2. MERRA Data

Near-surface energy budget and atmospheric variables were obtained from MERRA products [*Bosilovich et al.*, 2011; *Cullather and Bosilovich*, 2011, 2012; *Rienecker et al.*, 2011]. Data were obtained for a 108 day period from 15 March to 30 June capturing the melt seasons between 2003 and 2011. All MERRA variables were aggregated from hourly to daily, though diurnal temperature range was derived from hourly 2 m temperature data. MERRA is run on a 1/2° latitude by 2/3° longitude global grid with 72 hybrid-sigma vertical levels to produce analysis at 6 h intervals covering the modern satellite era from 1979 to the present. This program is generated with version 5.2.0 of the Goddard Earth Observing System atmospheric model and data assimilation system. It is coupled to the Community Radiative Transfer Model for radiance assimilation, and coupled to a catchment-based hydrologic model and a multilayer snow model for hydrological processes, with the specific goal of improving the representation of water cycle processes in analyses. These fields are forced by the atmospheric model, with inputs assimilated from a wide range of remote sensing (primarily satellite) observations in addition to nonhydrologic surface observations.

MERRA has been evaluated extensively since its release [e.g., *Reichle et al.*, 2011; *Robertson et al.*, 2011; *Kennedy et al.*, 2011, *Zib et al.*, 2012], including in the Arctic [*Cullather and Bosilovich*, 2011, 2012; *Liston and Hiemstra*, 2011]. Given MERRA's heavy reliance on satellite data, changes in the observing systems and the evolution of bias correction schemes over more than 30 years pose a challenge to data integrity. The assimilation of the Special Sensor Microwave Imager in 1987 and Advanced Microwave Sounding Unit in 1998 provided some of the largest continuity challenges, but artifacts associated with their introduction were found to affect energy and moisture budget continuity mostly at lower latitudes and over the ocean [*Bosilovich et al.*, 2011; *Robertson et al.*, 2011]. Clouds in MERRA have generally been found to be optically weaker resulting in negative biases in water vapor and downwelling LW radiation [*Bosilovich et al.*, 2011; *Kennedy et al.*, 2011], though a validation of MERRA cloud fraction at two Arctic stations compared more favorably than the four other reanalysis products in the study [*Zib et al.*, 2012]. While the melt season can often pose the largest challenge to reanalysis surface fluxes due to rapidly changing albedo [*Cullather and Bosilovich*, 2011], MERRA's energy transport terms have validated reasonably well at the surface [*Cullather and Bosilovich*, 2012] with some negative flux biases likely due to cloud fraction and cloud properties [*Zib et al.*, 2012]. Additionally, many of the largest issues found in MERRA's evaluation do not apply to the variables or levels of the atmosphere used in this study [*Kennedy et al.*, 2011].

Eastern Pacific Oscillation (EPO) index data were obtained from the National Oceanic and Atmospheric Administration's Earth System Research Laboratory. A 3 day moving average is used to calculate the EPO index to filter high-frequency variability. The index is not standardized, but 1 standard deviation is approximately 90 decameters (dam). The EPO has centers of action of 500 hPa height fields where values from 55 to 65°N, 160 to 125°W are subtracted from values from 20 to 35°N, 160 to 125°W. The positive phase of the EPO manifests itself primarily as a trough in the Gulf of Alaska and a ridge in the Central Pacific, with a secondary ridge near Hudson Bay. This results in the tendency for warmer air to be advected northward over western Canada into the southwestern part of the study area. While the EPO is a descriptive tool rather than itself a mechanism for initiating the melt season, it is useful in further exploring the large-scale dynamics that control the energy balance when snow begins to melt.

3.3. Attribution Methodology

Five atmospheric variables that best represent the spectrum of potential melt drivers were used in the attribution study of melt onset, including 2 m temperature, total convergence of energy into the atmospheric column, insolation, 850 hPa specific humidity, and LW CRE. LW CRE is the contribution of LW radiation from clouds and is obtained by subtracting surface-absorbed all-sky LW radiation from surface-absorbed LW radiation assuming a clear sky. Energy convergence is defined in terms of the remaining energy balance terms as

$$-\nabla \cdot \widetilde{F}_A \equiv R_{top} + F_{sfc} - \frac{\partial A_E}{\partial t}$$

where R_{top} is the downward radiative flux at the top of the atmosphere, F_{sfc} is the net surface energy flux (positive upward), and A_E is the total energy in the atmospheric column. Energy convergence is obtained using a combination of MERRA moist static energy fields following *Cullather and Bosilovich* [2012, Appendix].

Temperature is generally determined by all the other terms in the energy balance, so it is a useful synthesis of them [*Zhang et al.*, 1997]. Other factors influencing MOD that were either not accounted for or were not

Table 1. Summary of Data Preparation, Indicating for Each Melt Driver Whether an Anomaly was Used in Place of Absolute Values, and Over What Period (if Any) Data Were Averaged[a]

Melt Driver	Anomaly	Averaging Period
Insolation	Yes	None
LW CRE	No	None
Specific humidity	Yes	MOD ± 1 day
Temperature	Yes	MOD ± 1 day
Energy convergence	No	MOD ± 2 days

[a]An averaging period of "none" indicates that data only on the MOD were used.

relevant in this region include elevation (with associated slope and aspect influences), land cover, rain on snow events, katabatic winds, and turbulent heat fluxes. All turbulent fluxes were omitted in the attribution because their magnitude was found to be too small, generally under $5\,W\,m^{-2}$ for the daily mean.

Dominant controls on melt onset, i.e., melt attribution, were chosen based on their influence in the above energy balance and to account for the primary mechanisms by which energy is brought to the surface. All of these variables are largely interrelated, so melt can be attributed to more than one driver at once. Anomalies from the 33 year (1979–2011) mean were used for the attribution analysis except for LW CRE and energy convergence which used absolute values (Table 1). The time series of the 9 year mean of both these variables has a large variance, making their anomalies less meaningful. The averaging interval for each variable in the time period around MOD was chosen to best suit its ability to operate as a melt stimulus and reduce high-frequency noise when necessary (Table 1). For example, cloud cover tends to vary over shorter time scales than energy advection, so both LW CRE and insolation were not averaged beyond daily.

For all variables except energy convergence (see below), a threshold of $50\,W\,m^{-2}$ was chosen in a physically and empirically (e.g., time series analysis) based assessment of the magnitude necessary to perturb the system enough to initiate melt. For temperature and humidity anomalies, a linear regression was done with downwelling LW radiation anomalies around MOD to determine how much of an increase in these respective variables would result in an increase in $50\,W\,m^{-2}$ of incoming radiation, on average. The regression was done using only temperature values between −10°C and 10°C, the typical range of temperatures near melt onset. The regression results yielded 4°C for temperature and 1.3×10^{-3} kg/kg for specific humidity. The threshold for energy convergence was set at $150\,W\,m^{-2}$. In contrast to incoming SW and LW radiation at the surface, energy convergence is used both in heating the atmospheric column (dA_E/dt) and escaping to space (R_{top}). Thus, a conservative estimate of this threshold must be considerably greater than for incoming SW and LW radiation alone. The amount of advected energy reaching the surface varies considerably, but $150\,W/m^{-2}$ was chosen as an estimate with the caveat that the number of years attributed to energy convergence is subject to a higher range of uncertainty. Given these thresholds, the number of years that exceeded them were calculated for each variable and then averaged across each region; hence, resulting values for years are not typically whole numbers.

To examine the sensitivity of the melt attribution to the magnitudes of the threshold values, the attribution was done with a range of values from 25 to $75\,W\,m^{-2}$ for the energy balance variables, and 75 to $225\,W\,m^{-2}$ for energy convergence. This sensitivity study shows that the average change in attributed years for a $10\,W\,m^{-2}$ ($30\,W\,m^{-2}$ for energy convergence) change in threshold is generally under 1 year for all melt drivers, with no apparent regional variation in sensitivity (Table 2). Sensitivity is slightly higher for energy convergence and LW CRE and lower for specific humidity anomalies, but the difference is not enough to alter conclusions. Thus, this method is suitable to assess regional differences in dominant drivers for melt onset.

Table 2. Sensitivity Analysis of the Attribution Analysis to the Incoming Radiation Threshold, Performed in the Range of $25–75\,W\,m^{-2}$ ($75–225\,W\,m^{-2}$ for Energy Convergence) in Each Subregion[a]

Melt Driver	Region 1	Region 2	Region 3
Insolation	0.7	0.92	0.48
LW CRE	0.62	0.76	1.36
Specific humidity	0.72	0.32	0.6
Temperature	0.24	0.2	0.56
Energy convergence	0.74	1.06	0.90

[a]Units are 1 Yr/$10\,W\,m^{-2}$ (1 Yr/$30\,W\,m^{-2}$ for energy convergence).

4. Results

4.1. Algorithm Validation and Melt Climatology

Validation of the melt algorithm at Baker Lake and Yellowknife is provided using snow depth and maximum temperature data (Figure 2). In nearly every year, the melt algorithm indicates melt onset within a day of inferred onset (i.e., maximum temperature above freezing
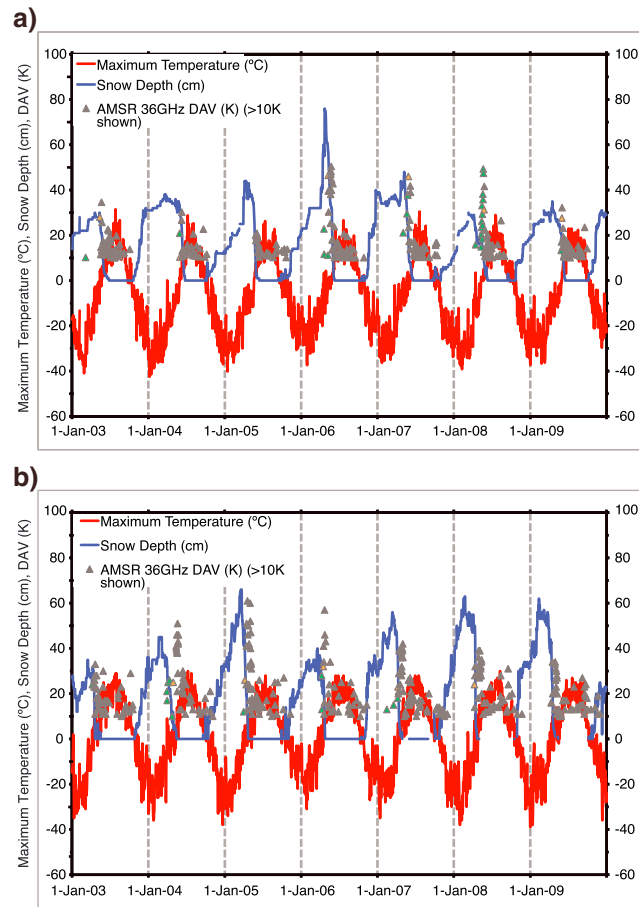
Figure 2. Time series of maximum temperature (°C) and snow depth (cm) with AMSR diurnal amplitude values (K) at the 36 GHz frequency overlaid for 2003–2009 at (a) Baker Lake, NU, and (b) Yellowknife, NT. The MOD is determined by a secondary algorithm, and the marker on this date is colored orange while any days with DAV > 10 K prior to this are colored green. DAV values greater than 10 K are displayed here even though only days when DAV exceeds 18 K are considered candidates for MOD.

accompanied by a decrease in snow depth). 2005 at Baker Lake is the only discrepancy, when the maximum temperature is between 0°C and 4°C for nearly a week with a large reduction in snow depth before the DAV increases over 18 K, while onset detection at Yellowknife has no such aberrations. The first date when DAV exceeds 18 K is not necessarily the MOD but becomes a candidate to be such when the onset algorithm is applied to mask early melt events. In 2006 and 2008 at Baker Lake and 2004 at Yellowknife there is an early melt event that is correctly ignored by the MOD algorithm; the DAV rises above its threshold, but not for enough days to indicate that the primary melt season is underway. In fact, the largest uncertainty in MOD may not be from melt detection methods themselves but simply in consistently extracting the onset of the primary melt season which can sometimes be relatively indistinct.

Snowmelt onset varies strongly over the study area dictated by latitude and longitude (Figure 3). Melt typically begins by 1 April near Region 1 and much of the boreal forest but not for another 2 months farther northeast toward Region 3 (Figure 3). Snow cover duration and snow water equivalent (SWE) have been assessed in other studies, showing a very similar spatial gradient from southwest to northeast

[*Brown et al.*, 2007]. *Wulder et al.* [2007] reported mean February SWE values from 80 to 110 mm across the southwestern third of the study area, while this sharply decreased to 40–60 mm in the tundra transition zone and less than 30 mm even farther to the northeast. The division of the current study area into three regions is motivated by this spatial distribution of MOD and associated hydrologic terms. A further understanding of the differences in melt season, particularly around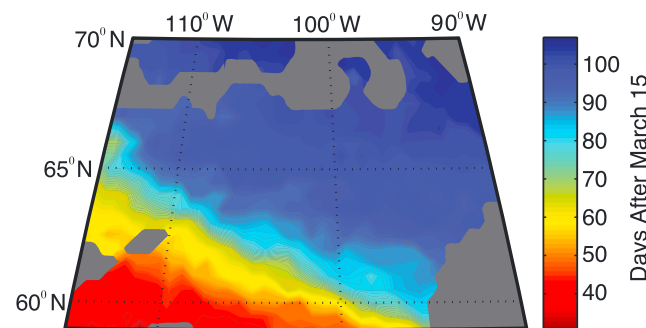 MOD, requires an understanding of the energy balance terms at the local scale in the context of the general synoptic pattern during this period.

Figure 3. The 2003–2011 mean melt onset date plotted in days after 15 March.

4.2. Energy Balance

Much of the motivation for choosing the extent of the three regions comes from the spatial differentiation in energy balance terms, primarily insolation and energy convergence (Figures 4a and 4b). The energy balance in all three regions is dominated by energy convergence, but with growing
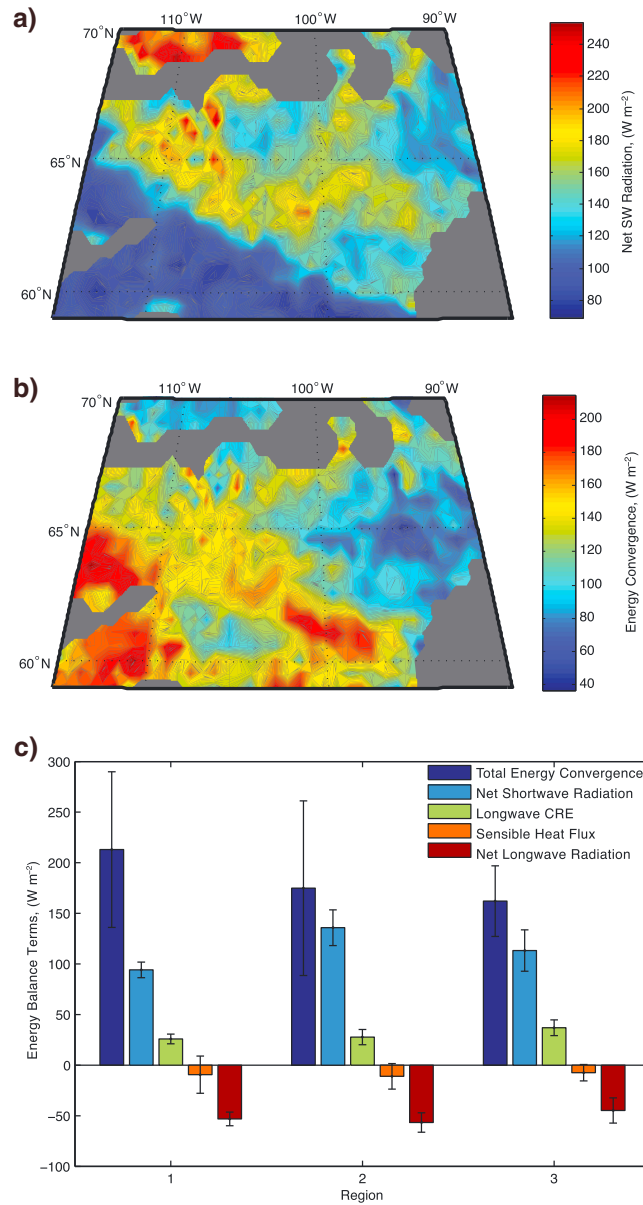
Figure 4. (a) Three day mean centered on MOD of 2003–2011 averaged net SW radiation and (b) energy convergence and (c) 2003–2011 mean values of the four primary components of the energy balance and the LW contribution from clouds in each region. A 3 day mean centered on the spatially averaged MOD for each region is used. Error bars are placed at 95% confidence intervals.

influence of shortwave (SW) radiation in the northern regions (Figure 4c). Energy convergence is used as a proxy for the advective energy of air masses, following *Aizen et al.* [2000]. Not all of this energy is available as melt energy at the surface; energy that advects into the atmospheric column both warms the column and is radiated in all directions primarily as LW radiation, including energy lost to space and the downwelling LW radiation considered in this surface energy balance. The energy balance in Figure 4 is dominated by SW radiation and energy convergence, whereas LW radiation and sensible fluxes are slightly negative (positive upward flux). A positive upward flux in LW radiation indicates that surface emission exceeds atmospheric downwelling of LW radiation. The typical LW contribution from clouds is generally insignificant relative to all incoming LW radiation, which ranges from approximately 220–270 W m^{-2} on average.

The largest differences regionally in the energy balance are in SW radiation and energy convergence terms. Region 1 exhibits less SW radiation due to the earlier melt date but also greater energy convergence, particularly relative to Region 3. There is also evidence for a different split in the net radiation balance between Regions 2 and 3, with slightly more LW radiation and LW CRE but less SW radiation in Region 3 than Region 2. This is consistent with observations of greater cloud cover and atmospheric moisture in Region 3 in the analysis below. Furthermore, downwelling LW radiation does not vary temporally nearly as much as SW radiation because many factors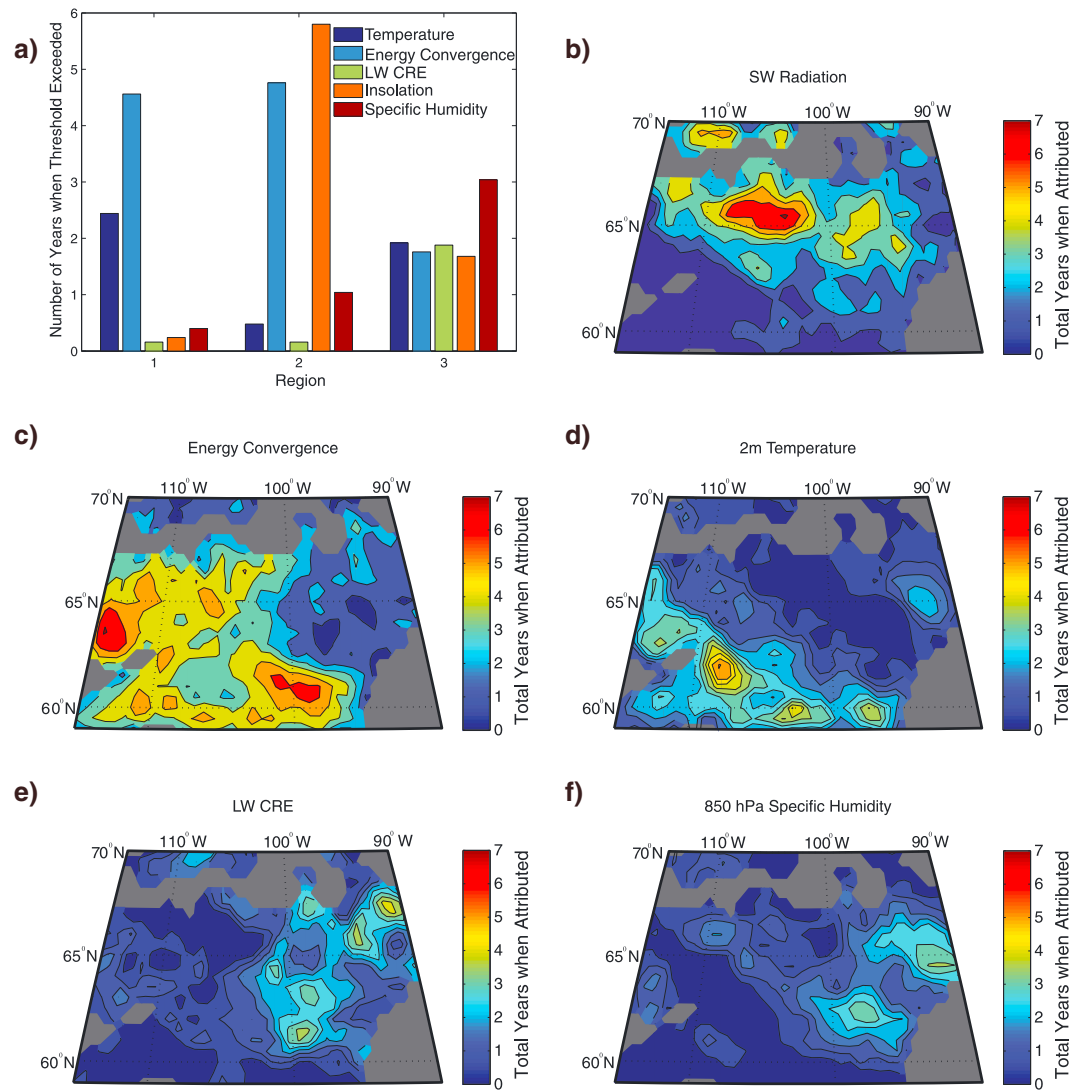 control atmospheric LW emission (e.g., cloud fraction, cloud base height, optical thickness, advected energy, and atmospheric thickness), whereas SW radiation fluctuates to first order only with cloud cover (at a constant latitude and Julian day). Therefore, the effect of cloud cover on the net surface LW radiation over periods of several days is reduced relative to the effect of increased SW radiation in their absence.

4.3. Melt Attribution

Strong regional variation in melt attribution variables around MOD closely follows variation found in the energy balance (Figure 5). Anomalies in insolation can be considered a melt driver in up to 6 years of the study period in the area surrounding Region 2 but in only a few years in Region 3 and never southwest of

Figure 5. Attribution of melt onset to melt drivers given as the number of years out of nine when the threshold is exceeded for each variable, (a) summarized by region and expressed spatially for (b) insolation anomalies, (c) convergence of total energy, (d) temperature anomalies, (e) LW CRE, and (f) specific humidity anomalies. Attribution threshold is 50 W m^{-2} for LW CRE and insolation, 150 W m^{-2} for energy convergence, 4 C for temperature, and 1.3×10^{-3} kg/kg for specific humidity. Data in map panels are smoothed with a convolution filter.

Region 1 (Figure 5a). Energy convergence accounted in part for three to six melt onsets in Regions 1 and 2 but for fewer than two in the tundra surrounding Region 3 (Figure 5b). Temperature anomalies exceeded 4°C in three to five melt seasons in the boreal forest but fewer than two seasons across much of the tundra, particularly around Region 2 (Figure 5c). LW CRE contributed to melt onset in an average of 2 years in Region 3 but was rarely a factor elsewhere (Figure 5d). Similarly, 850 hPa specific humidity anomalies could be considered a melt driver in about three melt seasons in Region 3 but in one or no melt seasons elsewhere, especially over the boreal forest (Figure 5e). Therefore, melt onset drivers appear to vary regionally, with energy convergence the dominant factor in Region 1, a large contribution from both energy convergence and insolation in Region 2, and mixed drivers in Region 3 with a greater influence from water vapor and clouds but less from energy convergence and insolation (summarized in Figure 5a).

Box plots of attribution terms show the largest regional differences to be in specific humidity anomalies and LW CRE (higher in Region 3 than elsewhere) and insolation (higher in Region 2 than elsewhere) (Figure 6). Energy convergence is generally lower in Region 3 but with high standard deviations in all regions
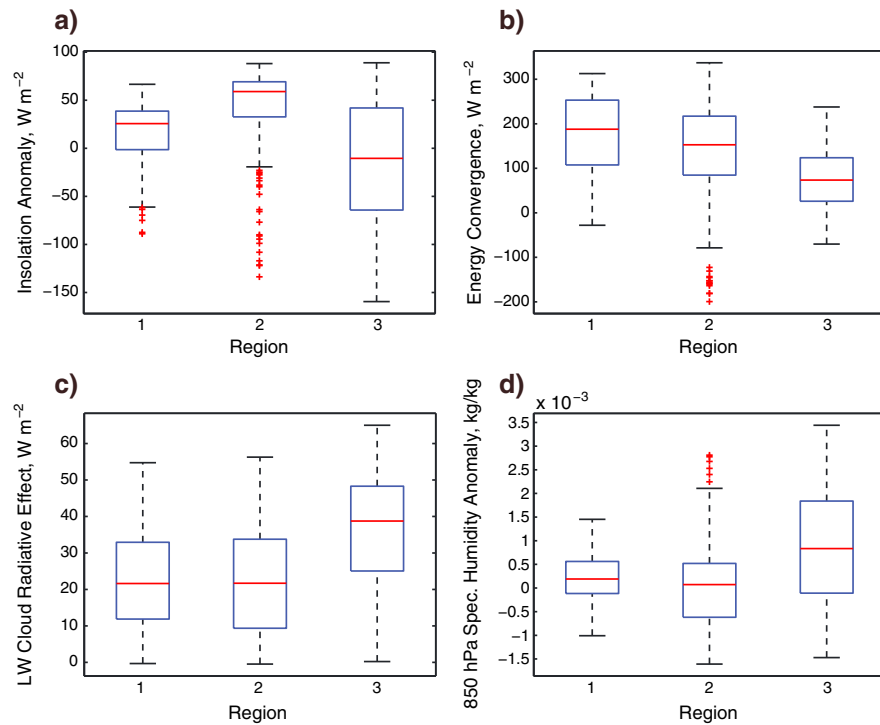
Figure 6. Box plots showing the 25th and 75th percentiles (box), median (red line), range (whiskers), and outliers (crosses) of (a) SW radiation anomalies, (b) convergence of total energy, (c) LW CRE, and (d) 850 hPa specific humidity anomalies.

(Figure 6b). Absolute values of LW CRE average only $20\,W\,m^{-2}$ in Regions 1 and 2, with few values over $50\,W\,m^{-2}$ anywhere, suggesting the significance of LW CRE as a melt driver may be relatively low (Figure 6c). 850 hPa specific humidity anomalies showed no sign preference in Regions 1 and 2, though the mean of 1 kg/kg in Region 3 is typically enough to increase downwelling LW radiation more than $40\,W\,m^{-2}$ (Figure 6d). Energy convergence exhibits the largest magnitude and temporal variability, with about half the data ranging between 150 and $250\,W\,m^{-2}$ in Region 1 compared to 25 to $125\,W\,m^{-2}$ in Region 3.

Temperature at MOD shows some of the largest variation across the entire study region. Daily mean temperature in the 3 day period surrounding MOD (Figure 7a) shows over 10°C in variation, with daily mean temperatures well below freezing in the southwest corner. The standard deviation of temperature in the broader period surrounding MOD (10 days; melt onset = day 7) in Regions 1, 2, and 3 is 5.2°C, 2.5°C, and 3.1°C, respectively, and the diurnal temperature range (not shown) varies from only 3–4°C in the northeast corner to over 12°C in the boreal forest. It is notable that daily means are used for temperature, which explains why melt begins at subzero temperatures. Much of the regional mean temperature difference is a result of differences in the diurnal temperature variation, which is not resolved with daily averages. Finally, daily mean regional temperatures in the week before and after MOD approaches 0°C in Regions 2 and 3 with a slight increase of a few degrees during this time, but the lower temperatures in Region 1 increase sharply around MOD (Figure 7b). Temperature anomalies around MOD are typically positive in Region 1, slightly negative in Region 2, and have no favored sign in Region 3 (Figure 7c). However, there is generally no strong bias toward positive temperature anomalies, indicating that temperature anomalies are not a reliable predictor of melt onset across the study area, particularly in Regions 2 and 3.

Results from this section provide support for the following observations: Region 1 is dominated by energy convergence and positive temperature anomalies, while Region 2 is controlled by energy convergence and SW radiation anomalies. Compared to the other regions, melt in Region 3 is more strongly controlled by water vapor anomalies and cloud-derived LW radiation. Diurnal temperature differences as well as those in temperature increase prior to MOD support the idea that melt is initiated by synoptic-scale events that can raise the temperature above freezing for at least a few days around Region 1, whereas the mean temperature
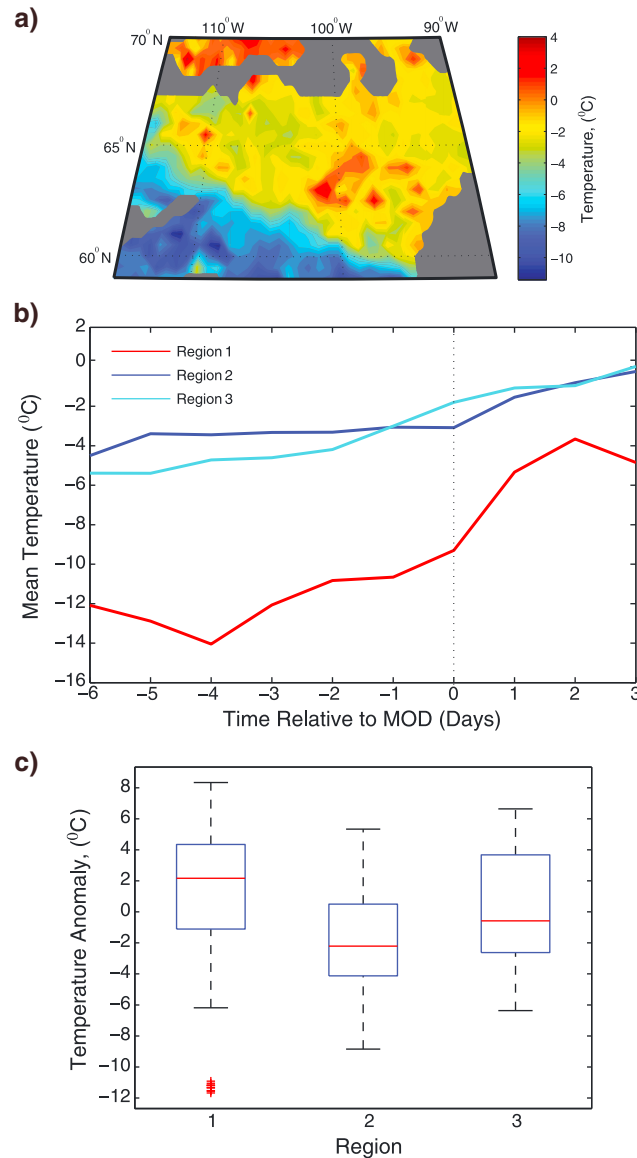
Figure 7. (a) Three day mean of 2 m temperature centered on MOD for each grid cell. (b) Time series of 2003–2011 mean 2 m temperature by region from the week before to the week after MOD. (c) Same as Figure 5 but for temperature anomalies.

farther into the tundra is warmer on average, likely from the greater amount of net radiation, and requires less stimulus to trigger melt onset.

4.4. Synoptic Overview

The three regions have widely different large-scale synoptic regimes shown by composite 500 hPa height anomaly fields and 2 m temperature anomalies at the time of MOD in each region, though Regions 2 and 3 bear more resemblance to each other than Region 1 (Figure 8). While average MOD in Regions 2 and 3 are very similar, individual years differ more with MOD being at least 1 week apart in 5 years out of 9. The different synoptic regimes help explain observed differences in several variables, particularly energy convergence. In Region 1, height anomalies are more pronounced during melt onset, showing a tendency for an upstream trough over Alaska. Such a trough generates higher heights over Region 1 with corresponding positive meridional wind anomalies advecting warmer air from the south (not shown). Positive 2 m temperature anomalies associated with this composite are 3–5°C (Figures 7c and 8a). Regions 2 and 3 (Figures 8b and 8c, respectively) have similar composite 500 hPa height anomaly fields for MOD but poorly defined synoptic features compared to Region 1. Relative to Region 1, Regions 2 and 3 have small positive height anomalies. In contrast to Region 1, Region 2 and 3's overall synoptic pattern is less conducive for meridional transport of heat, with temperature anomalies showing no sign preference.

Some of these dominant synoptic patterns are characteristic of regional modes of low-frequency variability (atmospheric teleconnections), and several of these teleconnections were tested for correlation with melt onset drivers. The synoptic pattern in Region 1 corresponds closely with the positive phase of the EPO (Figure 9). The EPO does exhibit some positive correlation over the 15 March to 30 June time period with temperature, LW radiation, and energy convergence. The highest positive correlation averaged over the 9 year period in all these variables occurs in Region 1 where the EPO index is highest during melt (temperature shown in Figure 9). There is no apparent relationship elsewhere in the study area, farther from the EPO center of action. During years when melt can be attributed to energy convergence, the mean EPO exceeds 1 standard deviation (90 m) in approximately the region bounded by the 0.2 correlation contour. Given the patterns in Figure 8, it is very likely that the correlation would be higher if the EPO index and 2 m temperature only around MOD were correlated. The short 9 year record precluded this, but it is still notable that more than 25% of variance in daily spring temperature from Region 1 to the southwest can be explained by the EPO. No
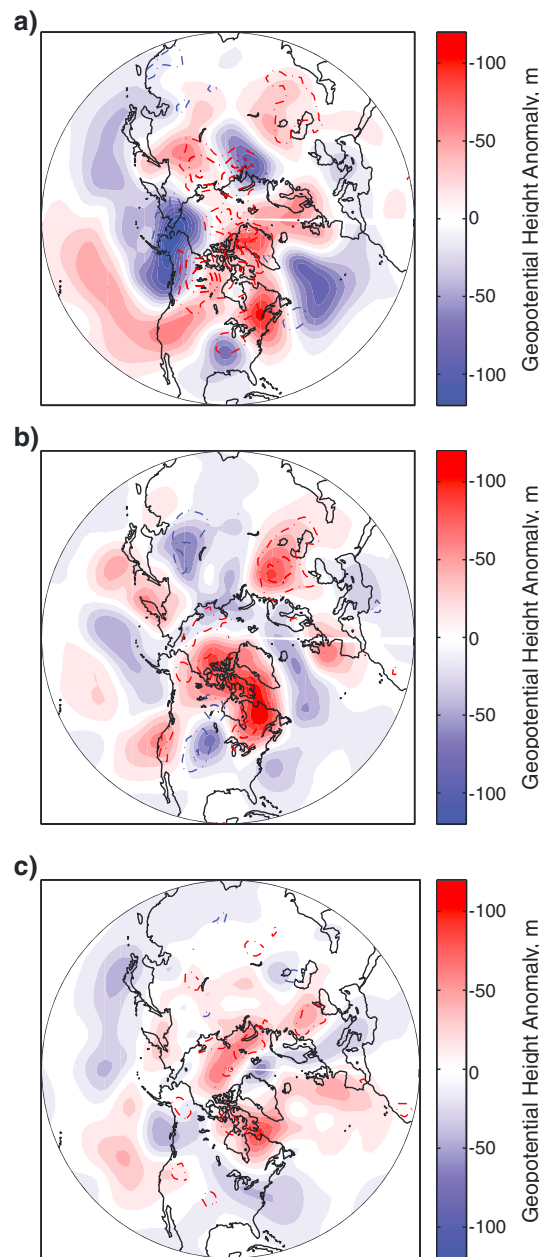
Figure 8. Composite 500 hPa height field anomaly maps from MERRA data at MOD spatially averaged for (a) Region 1, (b) Region 2, and (c) Region 3 each year from 2003 to 2011. Temperature anomalies are shown in dash-dotted lines in increments of 2°C with greater anomalies displayed as thicker lines.

significant correlation with temperature in the study area was found with the other dominant regional teleconnections, including the Arctic Oscillation, North Atlantic Oscillation, and Pacific North America pattern.

4.5. Analysis of Extreme Years

The earliest and latest MOD in each grid cell were obtained, and spatial means of similar atmospheric variables were calculated by region (Figure 10). Because extreme years were determined at the grid cell level, spatial averages in each region incorporate different years in some cases. The largest differences in most variables are differences across the region at MOD rather than differences between extreme years, and these differences are consistent with those found in the attribution analysis. Two meter temperature in Region 1 is 5–10°C lower than elsewhere, while energy convergence is nearly 50 W m^{-2} higher in Regions 1 and 2 than Region 3. Insolation and consequently net radiation are more than 50 W m^{-2} lower on average in Region 1 than elsewhere as a result of the earlier average melt date.

The greatest difference between early and late melts is in net radiation, derived mostly from more incoming SW radiation during late melts. There is a statistically significant difference in downwelling LW radiation and humidity in Region 1, with more water vapor in the earliest melts enhancing LW radiated to the surface. This difference is not apparent in the resultant net radiation, however, which is still dominated by the greater levels of insolation at the latest melt onset dates. Nearly every other variable is unchanged among extreme years, indicating that melt drivers typically remain regionally consistent regardless of when melt begins.

5. Discussion

In this study we demonstrate large differences in mean MOD in northern Canada, with a spatial pattern exhibiting a southwest-northeast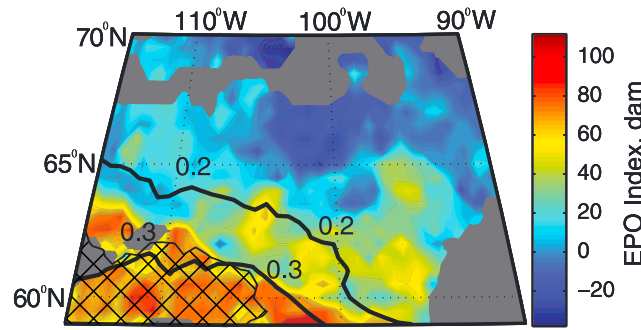 orientation. This matches the mean synoptic pattern with a trough near Hudson Bay, due in part to the topography of the Rocky Mountains and also the sharp boundary between boreal forest and tundra. This northwest-southeast oriented trough can be seen in 500 hPa height fields (manifested in 2 m temperature in Figure 1a) in all months and results in large differences in snowmelt timing as well as the corresponding energy balance terms across this relatively small region. The proximity to James and Hudson Bay does not appear to influence annual temperature variation, with Conrad's continentality index [*Conrad*, 1946] showing spatially uniform values in the 52–60 range. The large difference in surface land covers is not just a result of the climate but can strongly influence the spring melt process through its influence on surface albedo. The snow-albedo feedback is much stronger over bare tundra than over the

Figure 9. The 2003–2011 mean value of the EPO index at the 2003–2011 mean MOD in each grid cell. The 9 year mean Pearson product-moment correlation coefficient for the 15 March to 30 June time series of 2 m temperature and EPO index (contoured) shows a significant positive correlation across the southwestern part of the area. The hatched region indicates statistically significant correlation at $\alpha = 0.05$.

boreal forest, and this feedback is largest when the change in snow cover results in a large change in albedo [*Brown*, 2000]. While changes in shrub type and density across the warming Arctic's tundra transition zone can locally generate deeper snow depths and minor changes to the surface energy balance [*Sturm et al.*, 2001], the MERRA resolution is too coarse to capture these changes.

This part of Canada has been of additional interest recently due to some disagreement over spring snow cover duration among satellite data sets. *Wang et al.* [2005] evaluated the agreement in these data sets over tundra from 66°–74°

N, 80°–120° W and concluded that the NOAA weekly snow cover product exhibited a positive snow duration bias likely due to lower data coverage at high latitudes and enhanced cloud cover frequency during May and June, or to mixed pixels in the low-resolution IMS product prior to 1999. However, only years prior to the systematic change in this product to a higher resolution, daily, improved computer mapping system in 1999 were studied. Regardless of the cause, there is no reason to assume that there should be a trend toward earlier melt in this region. Here we have shown that the tundra near Hudson Bay is climatologically unique and may not respond strongly to enhanced energy advection that may be melting snow sooner elsewhere. The methodological nature and limited time span of this study cannot directly address the issue of data set quality but could provide further insight given that at least part of the discrepancy among data sets is likely rooted in snow-atmosphere interaction during the melt season. No IMS data are used in this study, but this discord has served as motivation to examine this region of Canada.

Composite 500 hPa anomalies show large differences in the hemispheric pattern during melt onset between Region 1 and Regions 2 and 3. There are stronger height anomalies at this time over Region 1 with a synoptic
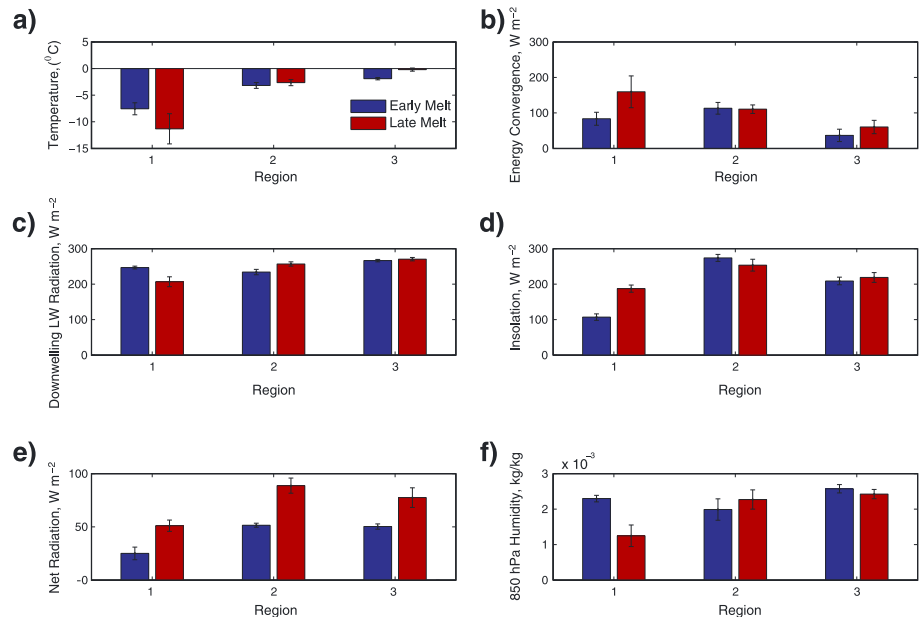

Figure 10. Spatial means and 95% confidence intervals during the year with earliest and latest MOD between 2003 and 2011 of (a) 2 m temperature, (b) energy convergence, (c) downwelling LW radiation, (d) insolation, (e) net radiation, and (f) 850 hPa specific humidity.

pattern that supports strong meridional wind anomalies and consequently large positive temperature anomalies. This pattern of height anomalies closely reflects the positive phase of the EPO, with its dominant mode over the North Pacific. This strong EPO signature during MOD in Region 1 underscores the importance of synoptic influences particularly in this area, specifically those with a North Pacific center of action.

Height anomalies are weaker and with a pattern that is less clear overall in Regions 2 and 3, though there is a stronger signal for ridging over Region 2. This is at least partially because these composite dates are later in the spring (late May/early June) when large-scale dynamics are not as strong when Rossby Waves become shorter and less amplified. Height anomalies over Region 3 show no discernible pattern and likely are instead a mix of disparate patterns over the 9 year period suggesting that the typical source of melt energy here is more local than a function of the synoptic pattern.

Mean temperatures prior to MOD in Region 1, relative to the remainder of the area, are (1) considerably lower but exhibit a greater increase, (2) more of a positive anomaly relative to mean temperatures for that Julian day, and (3) more variable on a daily basis given the higher standard deviation and much larger diurnal variation. Higher temperature anomalies are consistent with the lower mean temperatures in Region 1 because anomalies have to be more amplified to reach the freezing point, and this is also supported in Figure 7b where temperature rises more sharply when snow begins to melt.

In Region 1, energy advection is the dominant driver for melt onset shown by both its energy balance magnitude and number of days above the threshold. In contrast, LW CRE and 850 hPa specific humidity anomalies are very low, and SW radiation is not sufficient to generate anomalies on the scale of those in the remainder of the study area. Large temperature anomalies cannot be attributed to increased atmospheric moisture and clouds or greater amounts of SW radiation. Attribution variables and attributed days in Region 2 are similar to Region 1, only differing in mean insolation and temperature. Mean temperature anomalies are negative in Region 2 with strongly positive insolation anomalies, weak mean LW CRE, and neutral 850 hPa specific humidity anomalies. Melt in Region 3 appears to be more influenced by water vapor anomalies and cloud cover, which is also evident in 1000–500 hPa thicknesses and subsequently downwelling LW radiation (not shown), where it tends to be slightly higher than elsewhere. There is also less energy convergence in Region 3, indicating that melt relies less on advected energy and more on local-scale phenomena such as low clouds and local moisture sources. Finally, mean insolation is low relative to Region 2 at approximately the same latitude and Julian day, supporting the hypothesis that more energy here is derived from downwelling LW radiation from clouds and moisture than SW radiation. However, an assessment of mean low cloud fraction at MOD shows no significant difference between coverage over Regions 2 and 3 (though greater coverage than Region 1), so the observed differences in LW CRE and insolation anomalies may be accounted for by differences in cloud level or optical thickness, and it is possible that the two regions respond to these differently as melt drivers.

Advection of warm and moist air is commonly linked to snow ablation, particularly when there is no snow cover in the source region. *Ueda et al.* [2003] largely attributed snow ablation to energy advection from southwesterly winds over much of Eurasia, while *Aizen et al.* [2000] found that ablation in northern Russia was either augmented or delayed by the presence of snow cover to the south, which reduced the advective energy of air masses. Locally, the boundary between snow and bare vegetation (and snow patches at the smallest scale) can generate turbulent heat fluxes that advect melt energy over a snow-covered region [*Liston*, 1995; *Shook and Gray*, 1997] This has been found to enhance melt, though these processes are too small-scale to resolve with MERRA data. However, given the sharp boundary between boreal forest and tundra, and the resultant boundary in snow cover that often appears during the spring, it is conceivable that this mechanism commonly operates in this part of the study area, even though its relative significance is unknown.

Analysis of extreme years shows little difference among energy balance terms in the earliest and latest years (aside from SW radiation and its effect on net radiation), with again more of a regional difference supporting some of the conclusions discussed. *Iijima et al.* [2006] reached similar conclusions in an extreme year analysis at snow disappearance, finding that there was no significant difference between early and late values of surface air temperature, water vapor pressure, and LW radiation terms. While the sample size here ($n = 9$) is small, this does provide some evidence that the interannual variability in melt date is not dependent on the type of melt stimulus in this region.

6. Conclusions

This study analyzed the period of spring snowmelt onset between 2003 and 2011 in a climatologically diverse region of northern Canada west of Hudson Bay. Analysis indicates that there is more energy in the system further northeast by May and June, mostly from increased SW radiation closer to the solstice, but also less energy being advected into the atmosphere. This contrasts with less overall energy and lower temperatures to the southwest, requiring synoptic events and associated energy transport to provide the energy to initiate the primary melt season as well as the more frequent early melt events observed here. This is evident in composite 500 hPa height anomalies that are much more conducive to meridional energy transport. Sources of melt energy vary within the study region, with more energy typically being transported into Regions 1 and 2, a larger proportion from SW radiation in Region 2 and more from LW radiation derived from cloud cover and moisture in Region 3. While there is a greater increase in temperature in Region 1 prior to MOD, the lack of positive bias in temperature anomalies indicates that they are not a reliable predictor for MOD anomalies across the region. Finally, there is little difference in energy balance terms in extreme years, suggesting that the type of melt driver may not control interannual variability.

In a warming world with earlier melt onset dates, the results of this study can be informative in several ways. Snowmelt timing will likely respond differently to increased greenhouse gas forcing and Arctic amplification if there are large regional variations in melt drivers. Hemispheric studies addressing this research question should be prepared to downscale analysis to adequately resolve this variability. Additionally, some of these drivers and their associated feedbacks are predicted to change as the high latitudes change, such as atmospheric moisture and cloud cover, and energy advection [*Francis and Hunter*, 2007; *Graversen and Wang*, 2009; *Lu and Cai*, 2009; *Chen et al.*, 2011; *Ghatak and Miller*, 2013] while others, such as insolation, will remain constant. Being able to attribute melt onset to those drivers that are changing allows for better long-term prediction of melt season dynamics and the climatological processes influenced by snow cover and its feedbacks. A better understanding of the spring melt process and its sensitivity to a warming Arctic is critical to distributed hydrologic modeling, cryospheric feedback parametrization, and climate dynamics that extend beyond the Arctic into the entire hemisphere.

References

Aizen, E. M., V. B. Aizen, J. M. Melack, and A. N. Krenke (2000), Heat exchange during snow ablation in plains and mountains of Eurasia, *J. Geophys. Res.*, *105*(D22), 27,013–27,022, doi:10.1029/2000JD900279.

Aizen, V., E. Aizen, and J. Melack (2002), Estimation of the energy used to melt snow in the Tien Shan mountains and Japanese Islands, *Global Planet. Change*, *32*, 349–359.

Bamzai, A. S. (2003), Relationship between snow cover variability and Arctic oscillation index on a hierarchy of time scales, *Int. J. Climatol.*, *23*(2), 131–142, doi:10.1002/joc.854.

Bao, Z., R. Kelly, and R. Wu (2011), Variability of regional snow cover in spring over western Canada and its relationship to temperature and circulation anomalies, *Int. J. Climatol.*, *31*(9), 1280–1294, doi:10.1002/joc.2155.

Bintanja, R., and M. R. van den Broeke (1996), The influence of clouds on the radiation budget of ice and snow surfaces in Antarctica and Greenland in summer, *Int. J. Climatol.*, *6*(11), 1281–1296.

Brown, R., C. Derksen, and L. Wang (2010), A multi-data set analysis of variability and change in Arctic spring snow cover extent, 1967–2008, *J. Geophys. Res.*, *115*, D16111, doi:10.1029/2010JD013975.

Bosilovich, M. G., F. R. Robertson, and J. Chen (2011), Global energy and water budgets in MERRA, *J. Clim.*, *24*(22), 5721–5739, doi:10.1175/2011JCLI4175.1.

Brown, R. D. (2000), Northern Hemisphere snow cover variability and change, 1915–97, *J. Clim.*, *13*(1986), 2339–2355.

Brown, R. D., and D. A. Robinson (2011), Northern Hemisphere spring snow cover variability and change over 1922–2010 including an assessment of uncertainty, *Cryosphere*, *5*(1), 219–229, doi:10.5194/tc-5-219-2011.

Brown, R., C. Derksen, and L. Wang (2007), Assessment of spring snow cover duration variability over northern Canada from satellite datasets, *Remote Sens. Environ. Special Issue*, *111*(2–3), 367–381.

Camill, P. (2005), Permafrost thaw accelerates in boreal peatlands during late-20th century climate warming, *Clim. Change*, *68*(1–2), 135–152.

Chen, Y., J. R. Miller, J. A. Francis, and G. L. Russell (2011), Projected regime shift in Arctic cloud and water vapor feedbacks, *Environ. Res. Lett.*, *6*(4), 044007, doi:10.1088/1748-9326/6/4/044007.

Comiso, J. C., C. L. Parkinson, R. Gersten, and L. Stock (2008), Accelerated decline in the Arctic sea ice cover, *Geophys. Res. Lett.*, *35*, L01703, doi:10.1029/2007GL031972.

Conrad, V. (1946), Usual formulas of continentality and their limits of validity, *Trans. Am. Geophys. Union*, *27*, 663–664.

Cullather, R. I., and M. G. Bosilovich (2011), The moisture budget of the Polar atmosphere in MERRA, *J. Clim.*, *24*(11), 2861–2879, doi:10.1175/2010JCLI4090.1.

Cullather, R. I., and M. G. Bosilovich (2012), The energy budget of the Polar atmosphere in MERRA, *J. Clim.*, *25*(1), 5–24, doi:10.1175/2011JCLI4138.1.

Derksen, C., and R. Brown (2012), Spring snow cover extent reductions in the 2008–2012 period exceeding climate model projections, *Geophys. Res. Lett.*, *39*, L19504, doi:10.1029/2012GL053387.

Déry, S. J., and R. D. Brown (2007), Recent Northern Hemisphere snow cover extent trends and implications for the snow-albedo feedback, *Geophys. Res. Lett.*, *34*, L22504, doi:10.1029/2007GL031474.

Dong, X., G. G. Mace, P. Minnis, and D. F. Young (2001), Arctic stratus cloud properties and their effect on the surface radiation budget: Selected cases from FIRE ACE, *J. Geophys. Res.*, *106*(D14), 15,297–15,312, doi:10.1029/2000JD900404.

Dye, D. G. (2002), Variability and trends in the annual snow-cover cycle in Northern Hemisphere land areas, *Hydrol. Process.*, *16*(15), 3065–3077.

Dyer, J. L., and T. L. Mote (2006), Spatial variability and trends in observed snow depth over North America, *Geophys. Res. Lett.*, *33*, L16503, doi:10.1029/2006GL027258.

Foster, J. L., D. A. Robinson, D. K. Hall, and T. W. Estilow (2008), Spring snow melt timing and changes over Arctic lands, *Polar Geogr.*, *31*(3–4), 145–157.

Francis, J. A., and E. Hunter (2007), Changes in the fabric of the Arctic's greenhouse blanket, *Environ. Res. Lett.*, *2*, 045011, doi:10.1088/1748-9326/2/4/045011.

Ghatak, D., and J. Miller (2013), Implications for Arctic amplification of changes in the strength of the water vapor feedback, *J. Geophys. Res. Atmos.*, *118*, 7569–7578, doi:10.1002/jgrd.50578.

Graversen, R. G., and M. Wang (2009), Polar amplification in a coupled climate model with locked albedo, *Clim. Dyn.*, *33*(5), 629–643, doi:10.1007/s00382-009-0535-6.

Groisman, P. Y., T. R. Karl, R. W. Knight, and G. L. Stenchikov (1994), Changes of snow cover, temperature, and radiative heat balance over the Northern Hemisphere, *J. Clim.*, *7*(11), 1633–1656.

Hinzman, L. D., et al. (2005), Evidence and implications of recent climate change in northern Alaska and other Arctic regions, *Clim. Change*, *72*(3), 251–298, doi:10.1007/s10584-005-5352-2.

Iijima, Y., K. Masuda, and T. Ohata (2006), Snow disappearance in Eastern Siberia and its relationship to atmospheric influences, *Int. J. Climatol.*, *27*(2), 169–177, doi:10.1002/joc.1382.

Kennedy, A. D., X. Dong, B. Xi, S. Xie, Y. Zhang, and J. Chen (2011), A comparison of MERRA and NARR reanalyses with the DOE ARM SGP data, *J. Clim.*, *24*(17), 4541–4557, doi:10.1175/2011JCLI3978.1.

Knowles, K. (2006), *AMSR-E/Aqua Daily EASE-Grid Brightness Temperatures (Northern Hemisphere)*, NASA DAAC at the Natl. Snow and Ice Data Cent., Boulder, Colo.

Latifovic, R., Z. Zhi-Liang, J. Cihlar, and C. Giri (2002). Land cover of North America 2000, Natural Resources Canada, Canada Center for Remote Sensing, US Geological Service EROS Data Center.

Leathers, D. J., and D. A. Robinson (1997), Abrupt changes in the seasonal cycle of North American snow cover, *J. Clim.*, *10*(10), 2569–2585.

Lemke, P., et al. (2007), Observations: Changes in snow, ice and frozen ground, in *Climate Change 2007: The Physical Science Basis. Contribution of Working Group I to the Fourth Assessment Report of the Intergovernmental Panel on Climate Change*, edited by S. Solomon et al., Cambridge Univ. Press, Cambridge, U. K., and New York.

Liston, G. (1995), Local advection of momentum, heat, and moisture during the melt of patchy snow covers, *J. Appl. Meteorol.*, *34*(7), 1705–1715.

Liston, G. E., and C. A. Hiemstra (2011), The changing cryosphere: Pan-Arctic snow trends (1979–2009), *J. Clim.*, *24*(21), 5691–5712, doi:10.1175/JCLI-D-11-00081.1.

Lu, J., and M. Cai (2009), Seasonality of polar surface warming amplification in climate simulations, *Geophys. Res. Lett.*, *36*, L16704, doi:10.1029/2009GL040133.

Marsh, P., P. Bartlett, and M. MacKay (2010), Snowmelt energetics at a shrub tundra site in the western Canadian Arctic, *Hydrol. Process. 3620* (July), 3603–3620, doi:10.1002/hyp.7786.

Ohmura, A. (2001), Physical basis for the temperature-based melt-index method, *J. Appl. Meteorol.*, *40*(4), 753–761.

Pomeroy, J., and B. Toth (2003), Variation in surface energetics during snowmelt in a subarctic mountain catchment, *J. Hydrometeorol.*, *4*(4), 702–719.

Ramage, J. M., J. D. Apgar, R. A. Mckenney, and W. Hanna (2007), Spatial variability of snowmelt timing from AMSR-E and SSM/ I passive microwave sensors Pelly River, Yukon Territory, Canada, *Hydrol. Processes*, *21*, 1548–1560, doi:10.1002/hyp.6717.

Ramsay, B. (1998), The interactive multisensory snow and ice mapping system, *Hydrol. Processes*, *12*, 1537–1546.

Reichle, R. H., R. D. Koster, G. J. M. De Lannoy, B. A. Forman, Q. Liu, S. P. P. Mahanama, and A. Touré (2011), Assessment and enhancement of MERRA land surface hydrology estimates, *J. Clim.*, *24*(24), 6322–6338, doi:10.1175/JCLI-D-10-05033.1.

Rienecker, M. M., et al. (2011), MERRA—NASA's modern-era retrospective analysis for research and applications, *J. Clim.*, *24*(14), doi:10.1175/JCLI-D-11-00015.1.

Robertson, F. R., M. G. Bosilovich, J. Chen, and T. L. Miller (2011), The effect of satellite observing system changes on MERRA water and energy fluxes, *J. Clim.*, *24*(20), 5197–5217, doi:10.1175/2011JCLI4227.1.

Seager, R., D. S. Battisti, J. Yin, N. Gordon, N. Naik, A. C. Clement, and M. A. Cane (2002), Is the Gulf Stream responsible for Europe's mild winters?, *Q. J. R. Meteorol. Soc.*, *128*(586), 2563–2586, doi:10.1256/qj.01.128.

Semmens, K. A., J. Ramage, A. Bartsch, and G. E. Liston (2013), Early snowmelt events: Detection, distribution, and significance in a major sub-arctic watershed, *Environ. Res. Lett.*, *8*(1), 014020, doi:10.1088/1748-9326/8/1/014020.

Serreze, M. C., and J. A. Francis (2006), The Arctic amplification debate, *Clim. Change*, *76*(3–4), 241–264, doi:10.1007/s10584-005-9017-y.

Serreze, M. C., A. P. Barrett, A. G. Slater, M. Steele, J. Zhang, and K. E. Trenberth (2007), The large-scale energy budget of the Arctic, *J. Geophys. Res.*, *112*, D11122, doi:10.1029/2006JD008230.

Shi, X., P. Groisman, S. Dery, and D. Lettenmaier (2011), The role of surface energy fluxes in pan-Arctic snow cover changes, *Environ. Res. Lett.*, *6*, doi:10.1088/1748-9326/6/3/035204.

Shinoda, M., H. Utsugi, and W. Morishima (2001), Spring snow-disappearance timing and its possible influence on temperature fields over central Eurasia, *J. Meteorol. Soc. Jpn.*, *79*(1), 37–59.

Shook, K., and D. Gray (1997), Snowmelt resulting from advection, *Hydrol. Process.*, *11*, 1725–1736.

Sicart, J., and J. Pomeroy (2006), Incoming longwave radiation to melting snow: Observations, sensitivity and estimation in northern environments, *Hydrol. Processes*, *3708*, 3697–3708, doi:10.1002/hyp.6383.

Stone, R. S., E. G. Dutton, J. M. Harris, D. Longenecker, and W. Irrad (2002), Earlier spring snowmelt in northern Alaska as an indicator of climate change, *J. Geophys. Res.*, *107*(D10), 4089, doi: 10.1029/2000JD000286.

Sturm, M., J. P. McFadden, G. E. Liston, F. S. Chapin III, C. H. Racine, and J. Holmgren (2001), Snow – shrub interactions in Arctic tundra: A hypothesis with climatic implications, *J. Clim.*, *14*, 336–344.

Tedesco, M., R. Kelly, J. L. Foster, and A. T. C. Chang (2004), AMSR-E/Aqua Daily L3 global snow water equivalent EASE-Grids. Version 2, NASA DAAC at the Natl. Snow and Ice Data Cent., Boulder, Colo.

Tedesco, M., M. Brodzik, R. Armstrong, M. Savoie, and J. Ramage (2009), Pan Arctic terrestrial snowmelt trends (1979–2008) from spaceborne passive microwave data and correlation with the Arctic Oscillation, *Geophys. Res. Lett.*, *36*, L21402, doi:10.1029/2009GL039672.

Ueda, H., M. Shinoda, and H. Kamahori (2003), Spring northward retreat of Eurasian snow cover relevant to seasonal and interannual variations of atmospheric circulation, *Int. J. Climatol.*, *23*(6), 615–629, doi:10.1002/joc.903.

Vicente-Serrano, S. M., M. Grippa, T. Le Toan, and N. Mognard (2007), Role of atmospheric circulation with respect to the interannual variability in the date of snow cover disappearance over northern latitudes between 1988 and 2003, *J. Geophys. Res.*, *112*, D08108, doi:10.1029/2005JD006571.

Wang, L., M. Sharp, R. Brown, C. Derksen, and B. Rivard (2005), Evaluation of spring snow covered area depletion in the Canadian Arctic from NOAA snow charts, *Remote Sens. Environ.*, *95*(4), 453–463.

Wang, L., C. Derksen, R. Brown, and T. Markus (2013), Recent changes in pan-Arctic melt onset from satellite passive microwave measurements, *Geophys. Res. Lett.*, *40*, 1–7, doi:10.1002/grl.50098.

Wulder, M. A., T. A. Nelson, C. Derksen, and D. Seemann (2007), Snow cover variability across central Canada (1978–2002) derived from satellite passive microwave data, *Clim. Change*, *82*(1–2), 113–130, doi:10.1007/s10584-006-9148-9.

Zhang, T., K. Stamnes, and S. A. Bowling (1996), Impact of clouds on surface radiative fluxes and snowmelt in the Arctic and subarctic, *J. Clim.*, *9*(9), 2110–2123.

Zhang, T., S. A. Bowling, and K. Stamnes (1997), Impact of the atmosphere on surface radiative fluxes and snowmelt in the Arctic and Subarctic, *J. Geophys. Res.*, *102*(D4), 4287–4302, doi:10.1029/96JD02548.

Zhang, T., K. Stamnes, and S. A. Bowling (2001), Impact of the atmospheric thickness on the atmospheric downwelling longwave radiation and snowmelt under clear-sky conditions in the Arctic and Subarctic, *J. Clim.*, *18*(14), 920–939.

Zib, B. J., X. Dong, B. Xi, and A. Kennedy (2012), Evaluation and intercomparison of cloud fraction and radiative fluxes in recent reanalyses over the Arctic using BSRN surface observations, *J. Clim.*, *25*, 2291–2305, doi:10.1175/JCLI-D-11-00147.1.